Carbon 152 (2019) 898–908

Contents lists available at ScienceDirect

Carbon

journal homepage: www.elsevier.com/locate/carbon

Effect of the planar coil and linear arrangements of continuous carbon fiber tow on the electromagnetic interference shielding effectiveness, with comparison of carbon fibers with and without nickel coating

Hongtao Guan [a, b], D.D.L. Chung [a, *]

[a] Composite Materials Research Laboratory, Department of Mechanical and Aerospace Engineering, University at Buffalo, The State University of New York, Buffalo, NY, 14260-4400, USA
[b] School of Materials Science and Engineering, Yunnan University, Kunming 650091, PR China

ARTICLE INFO

Article history:
Received 19 April 2019
Received in revised form
24 June 2019
Accepted 26 June 2019
Available online 27 June 2019

ABSTRACT

The effect of macroscale planar arrangement (planar coil, unidirectional and crossply arrangements, with a gap between tow segments) of continuous polyacrylonitrile-based carbon fiber (7.0-μm diameter) 12 K tow on the electromagnetic interference shielding effectiveness for normal-incident unpolarized plane wave is reported at frequencies ranging from 200 to 2000 MHz. The planar coil configuration, which favors magnetic interaction, has not been previously reported for shielding with any material. For all arrangements, the total shielding effectiveness (SE_T) is dominated by the absorption loss (SE_A), whether the fiber is nickel-coated or not. The nickel coating (0.25-μm thick) increases SE_T from 2–6 dB to 13–26 dB for the planar coil configuration, but has little effect for the crossply/unidirectional configuration. Both SE_T and SE_A are greatly increased by the nickel coating, which also reduces SE_A's frequency dependence and increases the absorption's fractional contribution to shielding, particularly for the planar coil configuration below 1000 MHz (from 53%–78% to 83%–94%). The advantage of the crossply configuration over the unidirectional configuration is greater without the nickel coating. Increasing the tow size from 12 K to 24 K (with the gap decreased from 3.0 to 2.0 mm) raises SE_A for planar coil and unidirectional arrangements. The results agree essentially with electromagnetic theory.

1. Introduction

Due to their low density, high tensile strength and high tensile modulus, continuous carbon fibers are widely used for lightweight structures. As expected from their electrical conductivity, they are also effective for electromagnetic interference (EMI) shielding [1–4].

EMI shielding is increasingly needed, due to the abundance and sensitivity of electronics, which can malfunction in the presence of radio wave. In this sense, both electronics and radiation sources need to be shielded. Electromagnetic shielding can be contributed by reflection and absorption losses, which usually correlate closely to the electrical and magnetic characteristics of the shielding materials.

Although much work has been reported on a large variety of materials for EMI shielding, particularly nanomaterials in recent years, with the intended goal of developing materials that exhibit exceptionally high shielding effectiveness, comparative studies of materials that are related in the composition (e.g., with and without a certain type of material modification) and/or geometric configuration (e.g., different spatial arrangements of a material) have been inadequate. Study of the geometric configuration effect is particularly inadequate. In this work, the geometric configuration of concern is in the macroscale, in contrast to the large amount of prior work on the nanoscale configuration in nanostructures, such as those involving carbon nanotubes (including nanoscale coiled nanotubes) and graphene. Due to the large macroscale wavelength of the radio wave or microwave radiation, the macroscale configuration is highly relevant to EMI shielding considerations.

Geometric configurations involving metal meshes (mainly square meshes) of various macroscale sizes in the shielding material have been widely studied [5–8]. Geometric configurations involving linearly positioned parallel fibers (e.g., carbon fibers),

* Corresponding author.
E-mail address: ddlchung@buffalo.edu (D.D.L. Chung).
URL: http://alum.mit.edu/www/ddlchung

https://doi.org/10.1016/j.carbon.2019.06.085
0008-6223/

whether in unidirectional or crossply configurations, have also been investigated for EMI shielding [9–13]. However, the geometric configuration in the form of planar coil has not been previously reported in relation to EMI shielding, regardless of the type of material in the coil. The planar coil configuration for EMI shielding is to be distinguished from the planar coil configuration of an induction coil, which is a part of an electrical device for generating an intermittent high voltage from a direct current and is also used in induction heating.

In case of an unpolarized electromagnetic plane wave at normal incidence, as one travelling in a coaxial cable and used in this work, the electric field is radial and the magnetic field is circumferential. Thus, the planar coil configuration is potentially attractive for interaction of the shielding material with the magnetic field in the wave, while the linear configuration is attractive for interaction with the electric field in the wave. As a consequence, a comparative investigation of the effects of the planar coil and linear arrangements is attractive for shedding light on the nature of the interaction.

Carbon fibers differ from metals in their high degree of preferred crystallographic orientation, with the axial conductivity of a fiber being much higher than the transverse conductivity [1,9]. Due to the electrical anisotropy of each carbon fiber, and the directionality of the electric and magnetic fields in the electromagnetic radiation, the geometric configuration effect is expected to be more significant for carbon fiber structures than metal structures. However, prior work on the shielding effectiveness of carbon fiber structures has not addressed the effect of the macroscale spatial arrangement of the fibers, except for the effect of the linear arrangement of the fibers (e.g., unidirectional vs. crossply in the continuous fiber composite) [9,11,14].

Carbon fibers are available in the form of tows (with thousands or tens of thousands of fibers per tow). The large number of fibers in a tow is attractive for shielding, due to the large surface area enabled by the collection of microscale fibers. In contrast, the surface area is much lower for a metal wire in the macroscale. Linear arrangements of the tows are widely used as reinforcement in structural composites. The tows are conducive for other planar arrangements, such as the planar coil arrangement, which is not used for structural composites. Nevertheless, the planar coil arrangement of a tow is potentially attractive for EMI shielding and this is a focus of the investigation in this paper.

Although electromagnetic theory stemming from Maxwell's equations is well established, the science of EMI shielding is weak pertaining to the principles for the design of materials for shielding. The commonly used principle that is based on the electrical conductivity alone is not adequate for guiding this design. In spite of the large amount of reported empirical work for various shielding materials, a coherent set of principles for the material design has not been developed. The comparative studies mentioned above in relation to the composition and geometric configuration are important for strengthening the science base that will help the eventual realization of a coherent set of design principles.

In general, continuous carbon fibers are more effective than discontinuous carbon fibers in both shielding effectiveness [15] and reinforcement effectiveness [16], even though discontinuous fibers are lower in cost and amenable for composite fabrication by injection molding. Therefore, continuous carbon fiber composites are multifunctional structural materials that can provide the shielding function. For example, the shielding effectiveness (*SE*) of crossply continuous carbon fiber polymer-matrix composite of thickness 2.08 mm reaches 115 dB, as averaged over frequencies ranging from 0.3 MHz to 1500 MHz [17]. Unless noted otherwise, by *SE*, we refer to the total shielding effectiveness (SE_T), which is the sum of the absorption loss (SE_A) and reflection loss (SE_R).

The radiation that pertains to EMI shielding is most commonly in the form of an unpolarized plane wave at normal incidence. Due to the radial direction of the unpolarized electric field, a crossply fiber lay-up configuration gives superior shielding than a unidirectional fiber lay-up configuration [9,11,18]. In addition, a nonwoven carbon fiber fabric gives superior shielding than a woven carbon fiber fabric [19,20], in spite of the lower electrical conductivity [19], due to the random orientation of the fibers in the nonwoven fabric and the consequent enhanced interaction with the radiation.

Due to the circumferential direction of the magnetic field, a planar coil configuration of the fiber is expected to be attractive for magnetic interaction. Prior work has addressed shielding using carbon nanofibers/nanotubes that are coiled (three-dimensional, not planar) in the nanoscale [21]. However, fibers arranged in the form of macroscale coils are more in line with the long wavelength of the radio wave or microwave radiation and have not been previously investigated, whether for carbon fibers or other filamentary materials. Macroscale coils in the form of planar coils in the plane of the shield constitute a form of continuous fiber arrangement that can be achieved in a composite material.

The first objective of this paper is to investigate the effect of the macroscale planar coil configuration on the shielding effectiveness. Although the study is limited to carbon fibers, it is the first study of this configuration for shielding, regardless of the type of material.

The second objective is to investigate the effect of the continuous carbon fiber tow arrangement (macroscale geometric configuration) on the shielding effectiveness. The comparison of the effects of the linear arrangements (unidirectional and crossply) and planar coil arrangement allows a degree of decoupling of the electric field and magnetic field contributions to the shielding. Such decoupling is helpful for unraveling the science.

Carbon fibers are available in the form of metal-coated fibers, with the coating commonly obtained by electroplating. Since the metal is much more conductive than carbon, the electrical conductivity is much enhanced by the presence of the metal coating [22–26]. In case that the metal is magnetic, as in the case of nickel, which is ferromagnetic, the metal coating renders magnetic character to the fiber. The magnetic character of the fiber would enhance the shielding due to the interaction with the magnetic field component of the electromagnetic wave [27]. This enhanced magnetic interaction may alter how the abovementioned fiber arrangements affect the shielding. In other words, the effects of the planar arrangement and metal coating may be intertwined.

A study conducted by Kim et al. on the *SE* of nickel-coated carbon fiber polypropylene-matrix composite in the microwave frequency range shows that the composites prepared by different processes (namely injection molding, internal mixing and screw extruding) exhibit different EMI shielding performance characteristics, due to their different fiber arrangements (e.g., different degrees of fiber alignment) and hence different electrical and magnetic properties [28]. The shielding study of conductive silicone rubber filled with nickel-coated carbon fiber also shows that the alignment of the fibers in the matrix has great effect on *SE*, due to the effect of the alignment on the interaction with the magnetic field [28]. However, the effect of the nickel coating on the *SE* has not been addressed, due to the absence of comparison of the results for fibers with and without the nickel coating, and the absence of consideration of the absorption contribution (fractional contribution by absorption) to the total *SE*.

Carbon fibers shield mainly by the absorption of the radiation. The magnetic interaction, as promoted by the nickel coating, would add to the absorption [28–31]. For the purpose of understanding the mechanism of the shielding, this work includes determination of the absorption loss and reflection loss, whether the nickel

coating is present or not.

With consideration of the prior work and the open scientific questions regarding the inter-related effects of nickel coating and fiber arrangement on *SE*, the third objective of this paper is to unravel the nickel coating effect and the fiber arrangement effect in relation to the *SE*, absorption contribution and frequency dependence. This study involves the systematic comparison of the results for various combinations of fiber composition (with and without the nickel coating) and planar fiber arrangement (linear and coil).

The fourth objective of this work is to strengthen the science base for the design of materials for EMI shielding. For this purpose, this work investigates the effects of the material macroscale spatial arrangement (particularly the planar coil configuration, which has not been previously investigated for EMI shielding), composition-dependent magnetic character, composition-dependent conductivity, specimen thickness (as governed by the tow size) and frequency on the shielding characteristics. Furthermore, the consistency of these effects with electromagnetic theory is investigated. In spite of the large amount of prior research on the development of various materials for EMI shielding, relatively little attention has been given to the connection between the experimental results and electromagnetic theory [9].

2. Experimental methods

2.1. Materials and sample preparation

Two types of carbon fiber tows are studied. They are the uncoated carbon fiber (i.e., pristine carbon fiber, abbreviated PCF) and the corresponding nickel-coated carbon fiber (abbreviated NCCF). There are either 12,000 (12 K) fibers or 24,000 (24 K) fibers per tow. Unless noted otherwise, 12 K tows are used.

The nickel-coated continuous polyacrylonitrile (PAN) based carbon fiber is Tenax-J HTS40 A23 12 K 1420tex, with 12,000 fibers per tow, 1.3% sizing based on polyurethane resin, fiber diameter 7.5 μm (nickel coating thickness 0.25 μm, core carbon fiber diameter 7.0 μm), linear mass density 1420 tex, density 2.70 g/cm^3, electrical resistivity 7.5×10^{-7} Ω m, tensile modulus 215 GPa, tensile strength 2750 MPa, and tensile ductility 1.2% [32,33]. The fiber is provided by Teijin Limited (Japan). The nickel coating is deposited by the manufacturer on the carbon fiber by electroplating. The details of the electroplating process are proprietary. However, the process is likely conventional.

The corresponding uncoated continuous PAN-based carbon fiber that corresponds to the core carbon fiber of the nickel-coated carbon fiber is Tenax-E HTS45 E23 12 K 800tex, with 12,000 fibers per tow, 1.3% sizing based on epoxy resin, fiber diameter 7.0 μm, linear mass density 800 tex, density 1.77 g/cm^3, electrical resistivity 1.6×10^{-5} Ω m, tensile modulus 240 GPa, tensile strength 4500 MPa, and tensile ductility 1.9% [33–35]. The fiber is provided by Teijin Limited (Japan). This uncoated fiber is a high-strength standard-modulus aerospace-grade carbon fiber.

The PCF and NCCF are identical to those used in the recent work of this research group on the electric permittivity, piezoelectricity and piezoresistivity [36–38]. Compared to PCF, NCCF exhibits lower modulus, lower strength, lower ductility, and, obviously, higher density and lower resistivity. There is no twist in either type of fiber. The nickel-coated carbon fiber is silvery grey in color whereas the uncoated carbon fiber is black. The nickel coating is uniformly distributed on the surface of the carbon fiber, as shown by scanning electron microscopy [39].

The Rule of Mixtures for the density $\varphi_{Ni\text{-}C}$ of NCCF gives

$$\varphi_{Ni\text{-}C} = v_c\, \varphi_c + v_{Ni}\, \varphi_{Ni}, \quad (1)$$

where v_c and v_{Ni} are the volume fractions of carbon and nickel, respectively, and φ_c and φ_{Ni} are the densities of carbon and nickel, respectively. According to the fiber densities provided by the manufacturer, $\varphi_c = 1.770 \pm 0.005$ g/cm^3 and $\varphi_{Ni\text{-}C} = 2.700 \pm 0.005$ g/cm^3. The density of nickel is $\varphi_{Ni} = 8.908 \pm 0.001$ g/cm^3 [40]. Obviously,

$$v_c + v_{Ni} = 1. \quad (2)$$

The combination of Eqs. (1) and (2) gives $v_c = 0.870 \pm 0.002$, which is close to the geometric value of $v_c = 0.871 \pm 0.026$ calculated from the carbon fiber core diameter (7.00 ± 0.05 μm) and the nickel coating thickness (0.250 ± 0.005 μm). Between these two values of v_c, the value of 0.870 ± 0.002 is more accurate.

Different macroscale planar arrangements (Arrangements 1 and 2) are used in a comparative study to investigate the influence of the planar arrangement on the shielding effectiveness. Arrangement 1 (Fig. 1(b)) involves the tow in the form of a planar coil (or planar spiral), with the tow being continuous throughout the coil. Arrangement 2 (Fig. 1(c)) involves the tow in the form of parallel straight lines, with the tow being continuous between one line and the adjacent line at the proximate ends of the two lines. Either arrangement is achieved by manually attaching the tow to both sides of an annular-shaped piece of ordinary writing paper using ordinary adhesive tape, which is positioned above the tow, with the tow between the tape and paper (Fig. 1(d)). The center-to-center distance between the adjacent tow segments (whether the segments correspond to the windings in the coil in Arrangement 1, or parallel segments in the linear configuration of Arrangement 2) is 5.0 mm. In case of Arrangement 2, the attachment of the tow to the paper is followed by cutting away the parts of the tow within the central circle of the annular piece of paper. After the cutting, the tow is not continuous across the central circle.

The effect of the tow size (12 K *vs.* 24 K) is studied for the case of PCF only. The center-to-center distance between the adjacent tow segments is 5.0 mm for both 12 K and 24 K samples. The width of a tow is 2.0 mm and 1.5 mm for 12 K and 24 K, respectively. The gap between the proximate edges of the adjacent segments of the tow is 3.0 mm and 2.0 mm for 12 K and 24 K, respectively. The tow thickness in the direction perpendicular to the plane of the arrangement is 1.30 ± 0.05 mm and 2.50 ± 0.05 mm for 12 K and 24 K, respectively.

There are two versions of Arrangement 2, labeled Arrangement 2A and Arrangement 2B. They correspond to the direction of the tow being 0° or 90° apart on the two opposite sides of the paper. The 0° case is referred to as Arrangement 2A and is also described as being unidirectional. The 90° case is referred to as Arrangement 2B and is also described as being crossply.

The fiber volume fraction, as calculated based on the tow length, tow size and thickness, is higher for Arrangement 1 than Arrangement 2A/2B. For the same arrangement, the fiber volume fraction is higher for 24 K than 12 K. For Arrangement 1, the volume fraction is 13.6% and 16.6% for 12 K and 24 K, respectively. For Arrangement 2A/2B, the volume fraction is 11.8% and 14.4%, for 12 K and 24 K, respectively.

The writing paper used as the substrate for attaching the tow is annular in shape, with inner diameter 32 mm and outer diameter 96 mm. The inner and outer circular edges of each assembled sample are covered with silver paint in order to assure that an intimate contact occurs between the sample and the inner and outer conductors (via EMI gaskets in the form of O-rings) of the EMI testing fixture, which is described in Sec. 2.2.

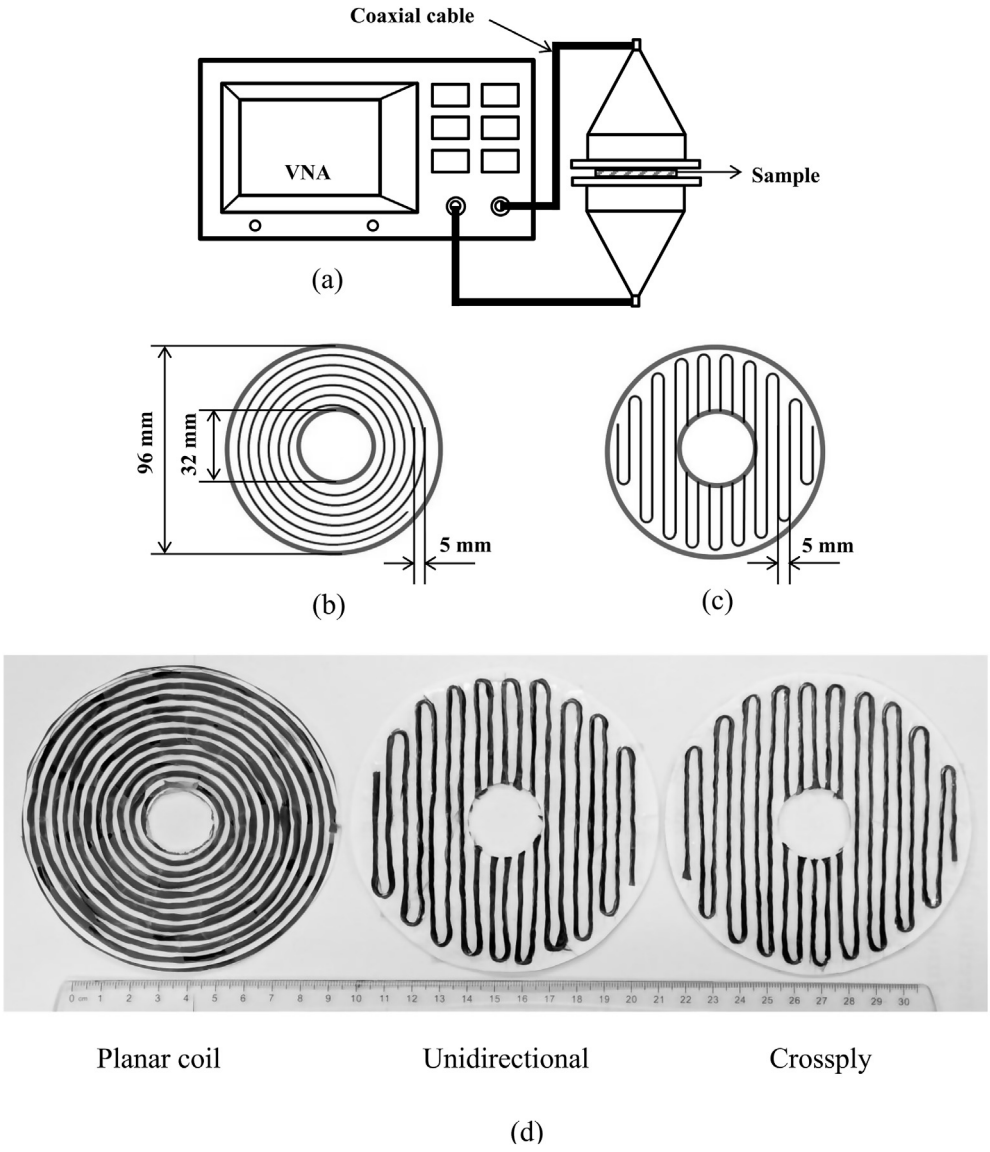

Fig. 1. Schematic illustrations of (a) the EMI shielding testing set-up involving a vector network analyzer (VNA), (b) Arrangement 1, and (c) Arrangement 2, with 5 mm being the center-to-center distance between adjacent tow segments. (d) The optical photograph of the specimens corresponding to the three planar arrangements, along with a ruler with major divisions in centimeters. The backside of the crossply arrangement is hidden from the view in (d), so the photos appear to be identical for the crossply and unidirectional arrangements in (d).

2.2. EMI shielding testing methods

The EMI shielding effectiveness (SE_T) for each sample is measured by using a vector network analyzer (VNA, TTR506A, Tektronix, Inc., 100 kHz–6 GHz, >122 dB dynamic range, <0.008 dB RMS trace noise) and the Coaxial Cable Method in the frequency range of 200 MHz−2000 MHz, as illustrated in Fig. 1(a). The sample is fastened between the two halves of the testing fixture by bolts under a controlled torque. Each of the two halves is a horn with inner and outer metal conductors that resemble an expanded coaxial cable, as illustrated in Fig. 1(a). The SE_T, SE_A and SE_R can be obtained from the scattering parameters (S parameters, namely S_{11} and S_{21}) through the equations [41],

$$SE_T = -10\log(P_t/P_0) = -10\log(T) = -10\log|S_{21}|^2 \quad (3)$$

$$\begin{aligned} SE_R &= -10((P_0 - P_r)/P_0) = -10\log(1-R) \\ &= -10\log\left(1-|S_{11}|^2\right) \end{aligned} \quad (4)$$

$$SE_A = SE_T - SE_R - SE_M \quad (5)$$

where P_0, P_r and P_t are the input power, reflected power and transmitted power, respectively, as is illustrated in Fig. 2. The T and R are the fraction of the input power that is transmitted and the fraction of the input power that is reflected, respectively. SE_M represents the shielding caused by the multiple reflection in the material. In practical application, SE_M is usually negligible when $SE_T \geq 15$ dB. Thus, SE_A can be obtained as

$$SE_A = SE_T - SE_R = -10\log[T/(1-R)] \quad (6)$$

The reflection contribution and absorption contribution are defined as SE_R/SE_T and SE_A/SE_T, respectively. In other words, the

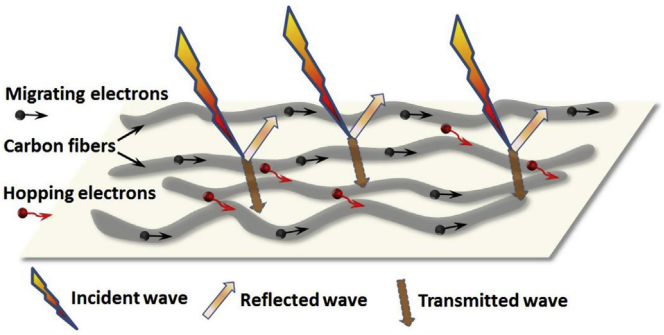

Fig. 2. Schematic illustration of the electromagnetic interaction with the carbon fibers. The electrons (mobile charge carriers) are indicated by circles (with the migrating electrons and hopping electrons distinguished). The electromagnetic wave (incident, reflected and transmitted) is indicated by the arrows. (A colour version of this figure can be viewed online.)

reflection contribution is the fraction of the SE_T that is due to reflection, and the absorption contribution is the fraction of the SE_T that is due to absorption.

Before the testing, the VNA and the measurement system are calibrated. The SOLT (short, open, load and through, 4-in-1) calibration kit (CALSOLTNM, Type-N, 9 GHz) is used for this purpose.

3. Results and discussion

The results are presented in terms of the effect of the planar arrangement (Sec. 3.1), the effect of the nickel coating (Sec. 3.2) and the effect of the tow size (Sec. 3.3). However, there is some overlap in Sec. 3.1 and 3.2.

3.1. Effect of the planar arrangement on the shielding effectiveness

Since the incident electromagnetic radiation is an unpolarized plane wave, it can be represented by its orthogonal electric and magnetic components. Under normal incidence, both electric and magnetic vectors are in the plane of the sample. Since the electric field vector is radial and the magnetic field vector is circumferential, Arrangment 1 is expected to allow more interaction with the magnetic field. Moreover, due to its much higher electrical conductivity, the NCCF coil (Arrangement 1) is expected to allow greater interaction with the electric field than the PCF coil (Arrangement 1). For Arrangement 1, both the magnetic and electrical interactions contribute to SE_A (and hence SE_T) for both PCF and NCCF. The results are described below in detail.

The SE_T and SE_A of Arrangements 1, 2A and 2B are shown in Figs. 3 and 4 for PCF and NCCF, respectively. Arrangement 2B gives much higher SE_T than Arrangement 2A, whether the nickel coating is present or not. This is expected, since the radiation is unpolarized.

Arrangement 1 gives lower SE_T than both Arragements 2A and 2B for PCF, and gives similar SE_T as Arrangement 2A for NCCF. In other words, the inferiority of Arrangement 1 to Arrangement 2 is clearer in the absence of the nickel coating. Since the coil configuration (Arrangement 1) is more effective than the linear configuration (Arrangement 2) for magnetic interaction, this suggests that the contribution of the magnetic interaction to shielding is small compared to that of the electrical interaction, though the magnetic interaction is increased in the presence of the nickel coating.

Concerning Arrangement 2A, since the fibers are arranged in a unidirectional pattern, SE_T reflects more interaction with the electric field than the magnetic field. Thus, Arrangement 2A has superior shielding performance than Arrangement 1 for PCF. For Arrangment 2B, due to its crossply configuration, it interacts with the electric field more than Arrangement 2A. As a consequence, Arrangment 2B gives much higher SE_T and SE_A than Arrangement 2A for both PCF and NCCF. This point is consistent with prior work on the comparison of unidirectional and crossply carbon fiber polymer-matrix composites, with the crossply composite giving higher shielding than the unidirectional composite [9]. In addition, it is consistent with prior work on the comparison of nonwoven and woven carbon fiber fabrics, with the nonwoven fabric giving higher shielding than the woven fabric [19].

For PCF, the absorption contribution is higher for Arrangement 2B than Arrangement 2A, and is comparable or higher for Arrangement 2B compared to Arrangement 1, as shown in Fig. 3(d). At frequencies below 1300 MHz, the absorption contribution for Arrangement 2B is higher than those of both Arrangement 2A and Arrangement 1, reflecting the dominance of electrical interaction in the absence of the nickel coating. For NCCF, the absorption contribution is comparable for all three arrangements above 600 MHz. However, below 460 MHz, the absorption contribution is greater for Arrangement 1 than Arrangement 2A or 2B, due to the relatively high degree of magnetic interaction at low frequencies for Arrangement 1 in the presence of the nickel coating.

For PCF, Arrangement 1 gives the lowest SE_T of about only 2−6 dB (Fig. 3(a)), whereas Arrangement 2B exhibits the highest SE_T that exceeds 32 dB for the entire frequency range (Fig. 3(a)). When the frequency is above 1000 MHz, SE_T reaches $\geq$35 dB for Arrangement 2B.

Both SE_T and SE_A increase greatly with the presence of the nickel coating on the carbon fibers, as shown by comparing Figs. 3 and 4. Comparison of Figs. 3(a) and 4(a) shows that the nickel coating increases SE_T from 2–6 dB to 13−26 dB for Arrangement 1, and from 33–37 dB to 35−39 dB for Arrangement 2B. Hence, the nickel coating enhanced SE_T significantly for Arrangement 1, but marginally for Arrangement 2A/2B. The effect of the nickel coating is addressed in more detail in Sec. 3.2.

3.2. Effect of the nickel coating on the absorption loss

Comparison of Figs. 3(b) and 4(b) shows that the nickel coating increases SE_A from 1–5 dB to 12−24 dB for Arrangement 1. This effect for Arrangement 1 is due to the enhanced magnetic interaction in the presence of the nickel coating. This enhancement is particularly significant below 600 MHz, due to the relatively intense magnetic interaction at low frequencies.

For Arrangement 2B, comparison of Figs. 3(b) and 4(b) also shows that the nickel coating increases SE_A significantly, particularly below 800 MHz. This is due to the enhanced electrical interaction in the presence of the nickel coating, and the particularly enhanced magnetic interaction at low frequencies.

For Arrangement 2A, comparison of Figs. 3(b) and 4(b) shows that the effect of the nickel coating on SE_A is small. This is probably due to the inherently low SE_A for this arrangement, whether nickel is present or not.

The nickel coating results in an interface between the coating and the carbon fiber surface, in addition to providing magnetic character, thus leading to a combination of electrical and magnetic interactions between the electromagnetic field and the fibers [42]. As a consequence, SE_A is increased by the nickel coating. In addition, conduction mechanisms have been invoked to explain the shielding effectiveness. In particular, the formation of a conductive network through the use of a conductive filler and the hopping of electrons across interfaces have been considered [43,44]. Since nickel has a much higher electrical conductivity than carbon fiber, it will favor the formation of a conductive network, thus enhancing SE_A. Moreover, electron hopping can occur from one fiber to

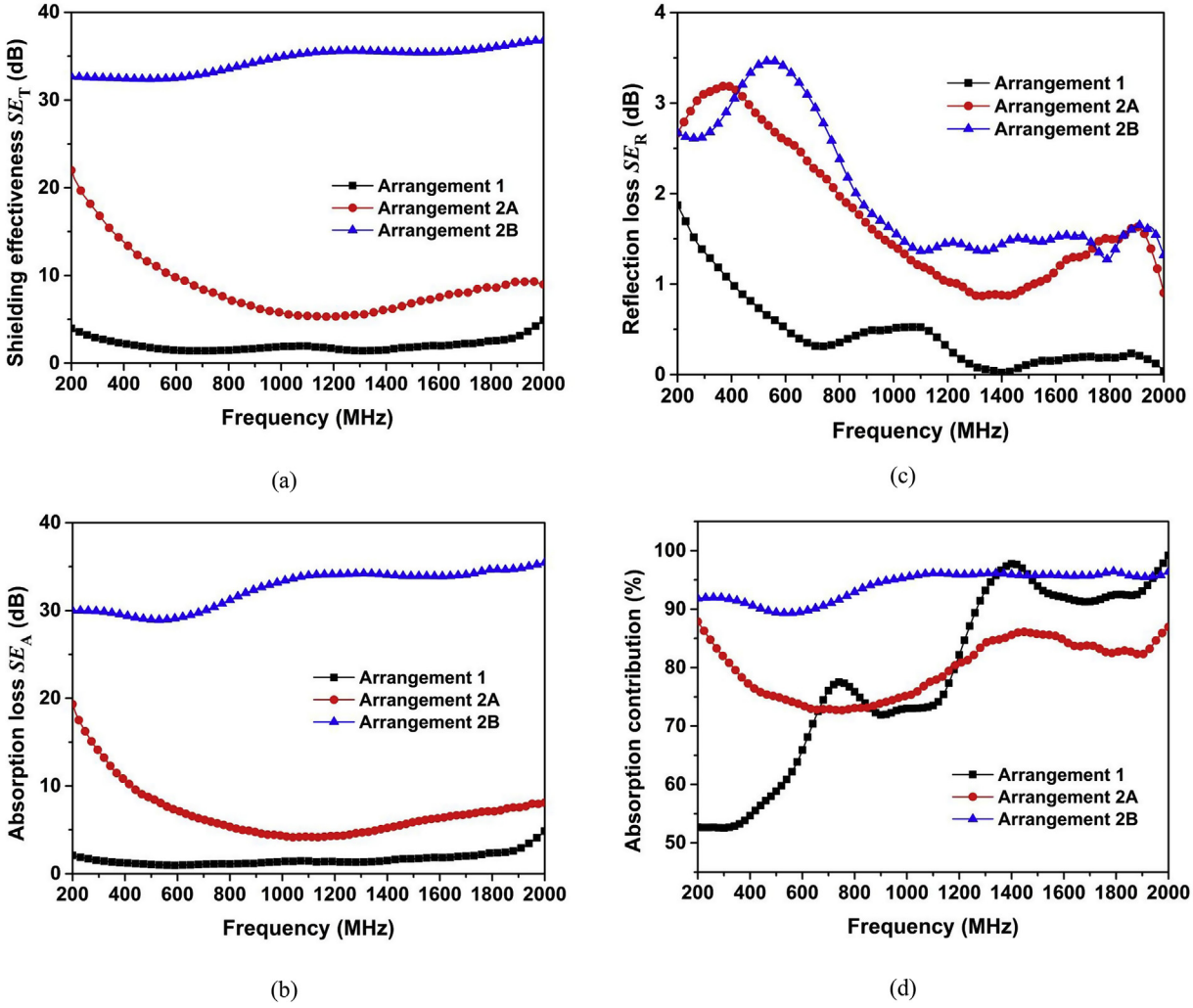

Fig. 3. Testing results for PCF with Arrangements 1, 2A and 2B. (a) Shielding effectiveness. (b) Absorption loss. (c) Reflection loss. (d) Absorption contribution. (A colour version of this figure can be viewed online.)

another through the fiber-fiber contacts within the same tow [45,46], thereby promoting conduction and contributing to the shielding effectiveness. In other words, the electrons move not only along the axis of a fiber, but also across from one fiber to an adjacent fiber. The temperature dependence of SE_A of CNT composites [43,44] also supports the importance of conduction to the shielding.

Comparison of Figs. 3(c) and 4(c) shows that the nickel coating increases SE_R significantly for Arrangement 1 at frequencies above 400 MHz. This is due to the enhanced electrical interaction, which is more significant at higher frequencies.

For Arrangement 2B, the presence of the nickel coating increases SE_R from the range 1.3–3.5 dB to the range 2.5–5.4 dB. For NCCF, SE_R increases monotonically with decreasing frequency below 800 MHz. For Arrangement 2A, the presence of the nickel coating increases SE_R only at frequencies below 100 MHz; above 1000 MHz, the effect of the nickel coating is relatively small. In relation to both Arrangements 2A and 2B, the nickel coating increases SE_R due to the high conductivity of nickel compared to carbon and the consequent small skin depth (δ) in the presence of the nickel coating. The skin depth is much smaller for nickel than carbon, so the nickel coating influences SE_R much less than SE_A.

The skin depth δ of the nickel coating in the frequency range studied is calculated based on the well-known equation

$$\delta = 1 \Big/ \sqrt{\pi f \mu_r \mu_0 \sigma} \tag{7}$$

where μ_r is the relative magnetic permeability of nickel, i.e., the permeability relative to that of vacuum μ_0 ($\mu_0 = 4\pi \times 10^{-7}$ H/m), σ is the electrical conductivity, and f is the frequency. It is thus found that the skin depth of nickel is in the range of 0.12–0.96 μm in the frequency range from 200 MHz to 2000 MHz, which is comparable to or larger than the nickel coating thickness of 0.25 μm. This means that the radiation penetrates essentially the complete thickness of the nickel coating.

Comparison of Figs. 3(d) and 4(d) shows that, for the entire frequency range, the nickel coating increases the absorption contribution from the range 53%–99% to the range 83%–98% for Arrangement 1, but has relatively little effects for Arrangements 2B and 2A. For frequencies below 1000 MHz, the effect of the nickel coating is even clearer; the nickel coating increases the absorption contribution from 53%–78% to 83%–94% for Arrangement 1, but has little effects for Arrangements 2A and 2B. For Arrangement 1 and frequencies below 1000 MHz, the effect of the nickel coating is particularly clear, with the nickel coating increasing the absorption contribution from 53%–78% to 83%–94%. In contrast, the nickel

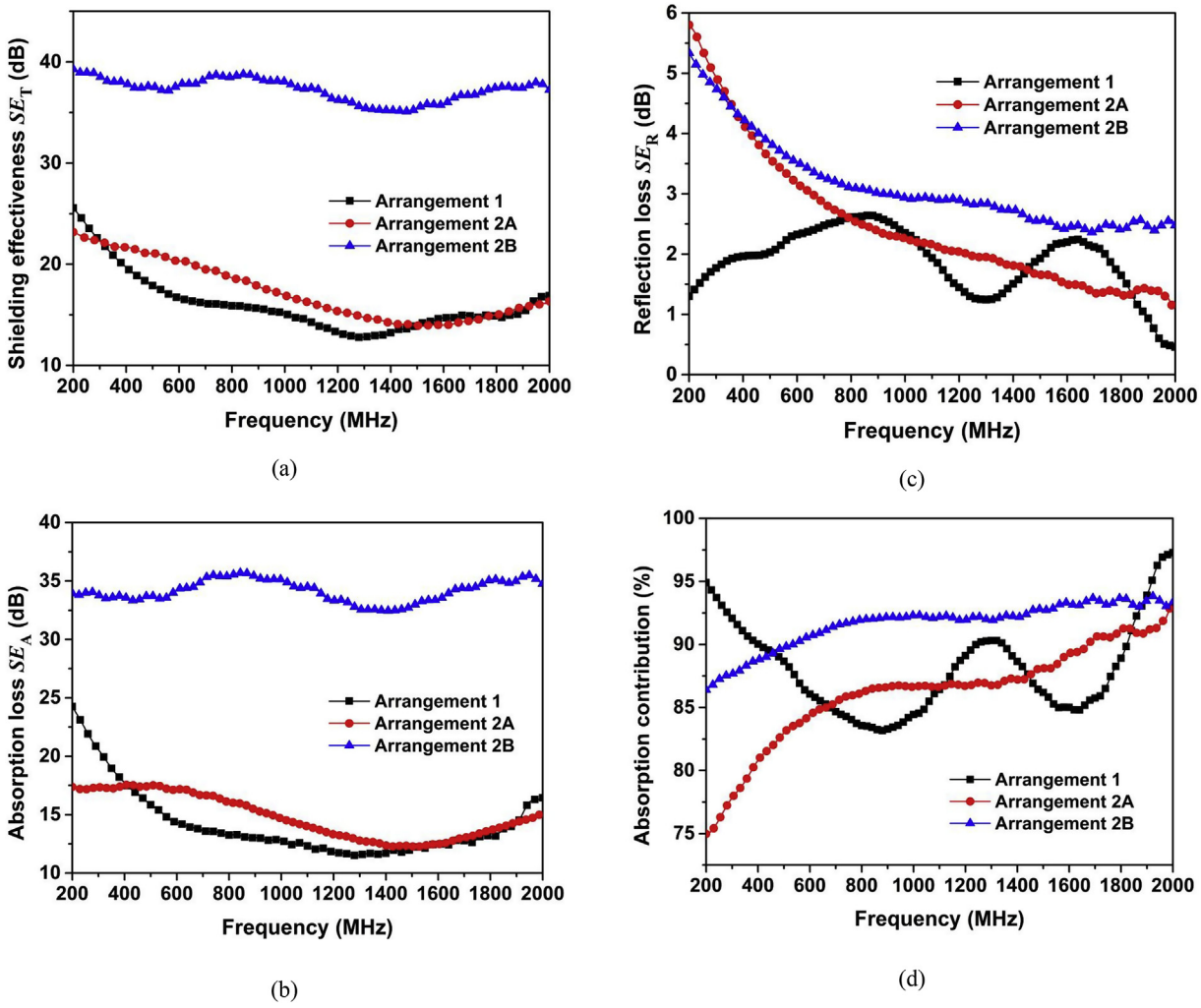

Fig. 4. Testing results for NCCF with Arrangements 1, 2A and 2B. (a) Shielding effectiveness. (b) Absorption loss. (c) Reflection loss. (d) Absorption contribution. (A colour version of this figure can be viewed online.)

coating changes the absorption contribution from the range 73%–89% to the range 75%–93% for Arrangement 2A, and from the range 89%–95% to the range 86%–93% for Arrangement 2B. This means that absorption dominates over reflection for both PCF and NCCF and that the nickel coating increases the absorption contribution for any of the three arrangements, with the absorption contribution increase due to the nickel coating being most significant for Arrangement 1, because of the enhanced magnetic interaction.

The present results are consistent with those of prior related work on polymers filled with nickel-coated carbon fiber or nickel-coated carbon nanofiber (nanofiber being originally known as filament) [28,47]. The SE_A of polypropylene-matrix NCCF composite in the microwave frequency range contributes up to about 85.1% of the total shielding (SE_T), due to the dielectric, magnetic and ohmic losses caused by the nickel coating [28]. A shielding study of acrylonitrile-butadiene-styrene (ABS) filled with carbon nanofiber (without metal coating) also demonstrates absorption domination of its SE_T, even in the high frequency range [47]. In a study of 3D printed carbon fiber (without metal coating) reinforced polylactic acid composites [48], the absorption domination is found to increase with increasing thickness, which is controlled through the multilayer printing.

The nickel coating reduces the frequency dependence of SE_A, as can be seen by comparing Figs. 3(b) and Fig. 4(b). Similarly, the nickel coating reduces the frequency dependence of SE_T, as shown by comparing Figs. 3(a) and Fig. 4(a). This phenomenon can be due to the decreased high-frequency permeability caused by the high electrical conductivity, due to Snoek's limit in the high-frequency permeability of magnetic materials [49].

The SE_A of a shielding material is given by the well-known equation [50,51] based on electromagnetic theory,

$$SE_A = 131.4t\sqrt{\mu_r \sigma_r f} \tag{8}$$

where t is the thickness of the sample, μ_r and σ_r are the relative magnetic permeability and the electric conductivity relative to copper, respectively. This means that SE_A increases with increasing frequency, in case that μ_r and σ_r are independent of the frequency.

Due to the high conductivity imparted by the nickel coating, μ_r of NCCF is expected to decrease substantially with increasing frequency. This trend is supported by the prior work on Mn–Zn and Ni–Zn spinel ferrites [49]. In contrast, for PCF, μ_r is approximately 1, with essentially no frequency dependence, due to its nonmangetic character. Therefore, in spite of the frequency dependence described by Eq. (8), the abovementioned trend causes the effect of the frequency on SE_A to be small for NCCF.

To further illustrate the effect of the nickel coating on the

absorption loss, the ratio α of SE_A of NCCF to that of PCF ($\alpha = SE_{A(NCCF)}/SE_{A(PCF)}$) is shown in Fig. 5(a). It reveals that the nickel coating plays a significant role in the absorption performance, especially for Arrangement 1. As shown in Fig. 5(a) for Arrangement 1, SE_A of NCCF is 3–16 times that of PCF, indicating the great effect of nickel coating on the absorption. For Arrangements 2A and 2B, α is much lower and is almost constant in the range of 1–4. The high SE_A of the NCCF coil compared to the PCF coil can be explained by Eq. (8), which indicates that SE_A is directly related to $\sqrt{\mu_r \sigma_r}$.

Due to the preferred orientation of the carbon layers in the carbon fibers along the fiber axis, the transverse conductivity of a fiber is much lower than the axial conductivity of the fiber. Recent work of this research group has shown that σ_r of a unidirectional carbon fiber polymer-matrix composite in the longitudinal direction is about 30 times higher than that in the transverse directions [9]. The linear arrangement in Arrangments 2A and 2B gives relatively high conductivity in the linear direction, with the conductivity stemming from the high axial conductivity of the fiber.

With the presence of a gap between the adjacent windings in the planar coil of Arrangement 1, the radial conductivity of the coil is very low – much lower than the transverse conductivity of the fiber. The low radial conductivity deters the interaction with the radial electric field in the electromagnetic radiation. Thus, SE_A of Arrangement 1 is dominated by the magnetic interaction. The ratio α for Arrangement 1 is high, ranging from 3 to 16 (Fig. 5(a)), with the value 12 at the lowest frequency (the frequency for the highest degree of magnetic interaction), mainly due to the increased μ_r in the presence of the nickel coating.

Based on Eq. (8),

$$\begin{aligned}\alpha &= \sqrt{\mu_r \sigma_r}(\text{NCCF})/\sqrt{\mu_r \sigma_r}(\text{PCF}) \\ &= (\sqrt{\mu_r}(\text{NCCF})/\sqrt{\mu_r}(\text{PCF}))(\sqrt{\sigma_r}(\text{NCCF})/\sqrt{\mu\sigma_r}(\text{PCF}))\end{aligned} \quad (9)$$

Due to the gap between the adjacent windings in Arrangement 1, the radial conductivity is essentially zero and hence the electrical interaction is negligible for both PCF and NCCF. Hence, for Arrangement 1, based on Eq. (9),

$$\alpha = \sqrt{\mu_r}(\text{NCCF})/\sqrt{\mu_r}(\text{PCF}). \quad (10)$$

The relative permeability of nickel (μ_{rNi}) ranges from 100 to 600, whereas that of pyrolitic carbon is 0.9996 [52]. Hence, the relative permeability of carbon is approximately equal to 1. The volume fraction of nickel in NCCF is 0.13 (Sec. 2.1). Thus the ratio $\mu_{r\,(NCCF)}/\mu_{r\,(PCF)}$ equals approximately 0.13 μ_{rNi}, which ranges from 13 to 78. With α ranging from 3 to 16 (Fig. 5(a)), $\mu_{r\,(NCCF)}/\mu_{r\,(PCF)}$ ranges from 9 to 256, according to Eq. (10). The ranges of 9–256 and 13–78 overlap substantially, thus supporting the notion that SE_A of Arrangment 1 is dominated by the magnetic interaction.

The SE_A of Arrangments 2A and 2B is dominated by the electrical interaction, due to their linear configuration, which results in high linear conductivity. The α for Arrangements 2A and 2B is low, ranging from 0.8 to 3.5 for Arrangement 2A and ranging from 1.0 to 1.2 for Arrangement 2B. This is because the electrical conductivity is substantial even in the absence of the nickel coating. Although the nickel coating enhances the conductivity, so that $SE_{A(NCCF)} > SE_{A(PCF)}$, α remains low. Based on Eq. (9), in the near absence of magnetic interaction for Arrangements 2A and 2B,

$$\alpha = \left(\sqrt{\sigma_r}(\text{NCCF})/\sqrt{\sigma_r}(\text{PCF})\right) = 4.62. \quad (11)$$

The value 4.62 is according to the known values of the fiber resistivities (Sec. 2.1). This value is not far from the observed values with the ranges mentioned above for these two arrangements (Fig. 5(a)). This supports the notion that SE_A of Arrangments 2A and 2B is dominated by the electrical interaction.

According to electromagnetic theory for unpolarized radiation, in the absence of magnetic interaction, the ratio β, defined as SE_A of Arrangment 2B to SE_A of Arrangement 2A ($\beta = SE_{A(\text{Arrangment 2B})}/SE_{A(\text{Arrangement 2A})}$), equals 4 [9]. As shown in Fig. 5(b), for both PCF and NCCF, $\beta > 1$ for the entire frequency range studied. This is due to the greater electrical interaction provided by Arrangement 2B compared to Arrangement 2A. The β ranges from 1.9 to 2.7 for NCCF and ranges from 1.5 to 8.2 for PCF, such that β for PCF is greater than β for NCCF for essentially the entire frequency range studied. The high β for PCF compared to NCCF is attributed to the higher conductivity provided by the nickel coating enhancing the electrical interaction, so that the difference between the performance of Arrangements 2B and 2A is diminished. The β is relatively independent of the frequency for NCCF, but varies much with the frequency for PCF. The cause for the frequency dependence of β for PCF is presently not completely clear. However, it appears that the nickel's enhancement of both electrical and magnetic interactions, which are significant at different frequencies, lessens the frequency dependence.

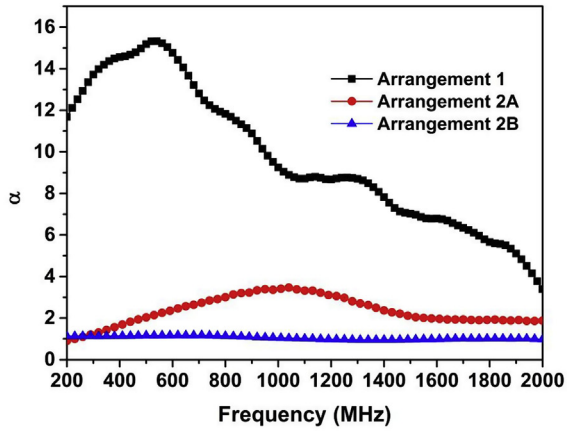

(a)

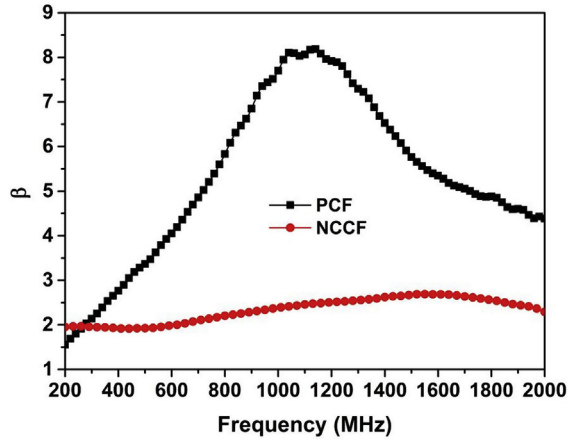

(b)

Fig. 5. Ratio of absorption losses. (a) α (ratio of NCCF to PCF) for Arrangements 1, 2A and 2B. (b) β (ratio of Arrangement 2B to Arrangement 2A) for PCF and NCCF. (A colour version of this figure can be viewed online.)

3.3. Effect of the tow size on the shielding effectiveness

The tow size effect is studied for PCT only. With 24 K tow instead

of 12 K tow, SE_T and SE_A are both enhanced for all three Arrangements, with the exception of Arrangement 2B below 500 MHz, as shown in Fig. 6(a). For Arrangement 2B below 500 MHz, the 12 K tow gives higher SE_T and SE_A than the 24 K tow. The cause of this unexpected behavior is presently unclear.

For Arrangement 1, 24 K gives SE_A that is about twice of that given by 12 K (Fig. 6(b)). For Arrangement 2A at frequencies above 600 MHz, 24 K also gives SE_A that is about twice of that given by 12 K (Fig. 6(b)). According to Eq. (8), the absorption loss should be proportional to the thickness. Therefore, this result is attributed to the fact that the thickness of the 24 K tow (2.50 ± 0.05 mm) is approximately twice of that of the 12 K tow (1.30 ± 0.05 mm). The deviation from a factor of 2 is partly because the fiber volume fraction is higher for 24 K than 12 K.

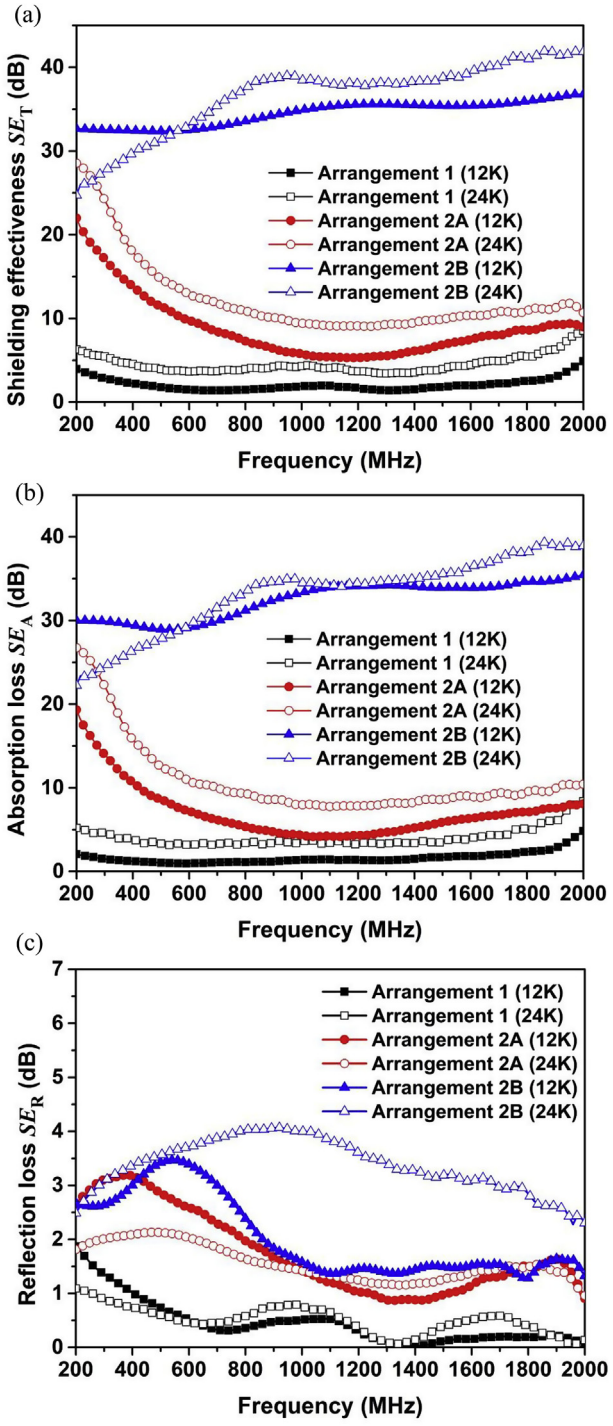

Fig. 6. Comparison of the *SE* results of PCF with 12 K and 24 K fiber tows. (a) Shielding effectiveness. (b) Absorption loss. (c) Reflection loss. (A colour version of this figure can be viewed online.)

For Arrangement 2B, due to its crossply configuration and the high electrical conductivity of the carbon fiber, the specimen can be considered as a bi-directional carbon fiber tow layer with periodically distributed square holes that are not covered by the tows. The size of the holes is 3.0 mm × 3.0 mm and 2.0 mm × 2.0 mm for 12 K and 24 K, respectively. Both sizes are much smaller than the wavelength (150–1500 mm) in the frequency range of 200 MHz–2000 MHz. It is known that, in case that the holes are less than 1/10 of the wavelength, the electromagnetic wave will barely transmit through the holes [53]. The transmission coefficient (T) of PCFs with the 12K/24 K tow is thus small and causes SE_T to be high. As a result, SE_T in case of Arrangement 2B is only slightly higher for 24 K than 12 K.

Based on Eq. (7), for the frequency range from 200 MHz to 2000 MHz, the skin depth δ of the carbon is in the range 0.09–0.29 mm. For both 12 K and 24 K tows, the specimen thickness is much larger than δ. Fig. 6(c) shows that, for both 12 K and 24 K tows, SE_R for Arrangement 1 is low for the entire frequency range, with similar values for 12 K and 24 K. The SE_R values for 12 K and 24 K are also similar for Arrangement 2A above 900 MHz. However, for Arrangement 2A, SE_R is lower for 24 K than 12 K at frequencies below 900 MHz; for Arrangement 2B, SE_R is higher for 24 K than 12 K for essentially the entire frequency range studied (Fig. 6(c)).

According to the electromagnetic shielding theory, SE_T can be expressed by the equation [54,55],

$$SE_T = 168 + 10\log(\sigma_r/f\mu_r) + 131.4t\sqrt{\mu_r\sigma_r f} \quad (12)$$

In Eq. (12), the last term on the right is SE_A (Eq. (8)) and the remaining two terms in front constitute SE_R. Due to the fact that SE_A increases with t whereas SE_R is independent of t, SE_T increases with t less significantly than SE_A. As a result, the difference between SE_T and SE_A (this difference being equal to SE_R) decreases with increasing t.

According to Eq. (8), at a given frequency, the ratio SE_A/thickness relates to $\sqrt{\mu_r\sigma_r}$. Table 1 thus compares the ratio SE_A/thickness at 1.0–1.5 GHz for various fibrous carbons. As shown in the prior work [9], for the same material composition, this ratio decreases with increasing thickness. Thus, the comparison shown in Table 1 is for the closest available thicknesses.

The ratio SE_A/thickness for PCF of this work is lower than that of the PCF polymer-matrix composite of prior work [9]. This difference is partly attributed to the much lower fiber volume fraction of the present work (Table 1). It is also partly attributed to the fact that the tow segments in this work are physically separate from one another by a gap, whereas the tows are adjacently positioned so that they are physically in contact in the polymer-matrix composite of the prior work [9]. The lateral contact between the tows helps the conduction in the longitudinal direction, due to the fact that there are defects in the fibers and the lateral contact allows the current to detour around defects [57]. Without the lateral contact between the tows, the detouring from one tow to another is not possible. This means that, in practice, the tow arrangement is preferably such that the adjacent tow segments touch one another, in contrast to the non-touching tow configurations of this work (Fig. 1). The non-touching configurations are used in this work in order to focus on the effect of the geometric arrangement.

For the same arrangement, the ratio SE_A/thickness is higher for NCCF than PCF. The values obtained in this work for PCF (23) and

Table 1
Comparison of SE_A/thickness at 1.0–1.5 GHz for various carbon materials. CNF = carbon nanofiber.

Material	Thickness (mm)	vol% fiber	SE_A/thickness (dB/mm)		
			Unidirectional	Crossply	Random
PCF composite [9]	0.957–0.966	49.5	14.3	64.6	/
PCF[a] (this work)	1.3	11.8	3.8	23	/
NCCF[a] (this work)	1.3	45.1	13	31	/
CNF mat [56]	2.86	6.1	/	/	16.4

[a] 12 K tow, Arrangement 2A/2B.

NCCF (31) in the crossply arrangement are higher than the value of 16.4 for carbon nanofiber (CNF) mat in which the CNF is randomly oriented [56]. This is partly because of the much lower CNF volume fraction (only 6.1%) and the larger CNF mat thickness (2.86 mm).

3.4. Applicability to carbon fiber polymer-matrix composites

Although this work concerns carbon fibers in the absence of a matrix, the findings are applicable to carbon fiber polymer-matrix composites. This is because the polymer matrix (akin to air) is typically essentially transparent to the radiation. The method of planar coil fabrication involving adhesive tape, as used in this work, will need to be modified for the fabrication of a polymer-matrix composite containing the planar coil. For example, in the composite fabrication, the planar coil arrangement of the tow may be secured by stitching to form a fiber preform, followed by infiltration with the polymer or its precursor.

4. Conclusion

The present work reports the effects of macroscale planar arrangements of continuous PAN-based carbon fiber (7.0-μm diameter without the nickel coating and 7.5-μm diameter with the nickel coating) on its EMI shielding performance for normal-incident unpolarized plane wave in the frequency range of 200 MHz–2000 MHz. The experimental results obtained using the Coaxial Cable Method are essentially in agreement with electromagnetic theory.

The fiber arrangements are planar coil, unidirectional and crossply arrangements, with the center-to-center distance between adjacent tow segments being 5.0 mm, and the gap between the proximate edges of adjacent tow segments being 3.0 mm and 2.0 mm for 12 K and 24 K tows, respectively. The inter-related effects of the planar arrangements, nickel coating (0.25-μm thick) and tow size (12 K and 24 K) on the *SE* are studied systematically for the first time. Of importance is that the planar coil arrangement, which favors magnetic interaction, has not been previously reported for EMI shielding with any material. For any of the arrangements, the total shielding (SE_T) is dominated by absorption (SE_A) rather than reflection (SE_R), whether the nickel coating is present or not.

For PCF, the planar coil configuration gives the lowest SE_T values of 2–6 dB, while the crossply configuration provides the highest values of 33–37 dB. Both SE_T and SE_A are greatly improved by the nickel coating for the planar coil arrangement, but not for the unidirectional or crossply arrangement. The nickel coating increases SE_T from 2–6 dB to 13–26 dB for the planar coil arrangement, but has little effect for the unidirectional or crossply arrangement. Moreover, for the planar coil configuration below 1000 MHz, the nickel coating increases the absorption contribution (by fraction) from 53%–78% to 83%–94%. The nickel coating also increases the absorption contribution for all three arrangements, from ≥50% to ≥85%. The nickel coating has more effect on the absorption contribution (particularly below 1000 MHz) for the coil arrangement than the linear arrangements, due to the magnetic interaction domination in case of the coil arrangement. Moreover, the nickel coating reduces the frequency dependence of SE_A for any of the three arrangements.

The ratio of SE_A of the crossply arrangement to that of the unidirectional arrangement is much greater for PCF than NCCF, due to the much higher electrical conductivity of NCCF compared to PCF. This means that the advantage of the crossply configuration over the unidirectional configuration is greater for PCF than NCCF.

The increase in the PCF tow size from 12 K to 24 K raises SE_A for planar coil and unidirectional arrangements, due to the increased specimen thickness and increased fiber volume fraction. However, for the crossply arrangement, the tow size has essentially no effect, due to the high degree of electrical interaction provided by this arrangement. The increase in the PCF tow size has little effect on the inherently low SE_R for the planar coil arrangement, but tends to decrease SE_R for the unidirectional arrangement and increase SE_R for the crossply arrangement.

The above results pertaining to carbon fibers indicate the following generalized conclusions concerning materials for EMI shielding that involves normal-incident unpolarized plane wave. These generalized conclusions serve to strengthen the science base for the design of materials for shielding. The parameters in the design include the material's geometric configuration (arrangement), magnetic character, conductivity and thickness.

(i) A planar coil arrangement attenuates electromagnetic radiation mainly through the magnetic interaction, so it gives good EMI shielding performance only for magnetic materials. On the other hand, the linear arrangements are dominated by electrical interaction with the electromagnetic field, and thus it is attractive for shielding using conductive materials, regardless of the magnetic character.

(ii) A magnetic material is attractive for promoting EMI shielding through increasing the absorption loss, due to the magnetic interaction, whether the arrangement is a planar coil configuration or a linear arrangement. The shielding improvement for a planar coil arrangement resulting from the magnetic character of the material is more significant compared to the corresponding shielding improvement for a linear arrangement.

(iii) A crossply configuration is more effective for shielding than a unidirectional configuration for unpolarized plane wave. The advantage of the crossply configuration over the unidirectional configuration is greater for shielding materials that are both non-magnetic and relatively low in the electrical conductivity.

(iv) The increase in thickness improves the shielding effectiveness for planar coil and unidirectional arrangements through increasing the absorption loss. However, for the crossply arrangement, in case of a material with substantial conductivity, both the magnetic coating and specimen thickness increase have little effect on the shielding performance, due to the high shielding inherently associated with the combination of substantial conductivity and crossply arrangement.

(v) High conductivity and magnetic character contribute to decreasing the dependence of the absorption loss on the frequency.

References

[1] D.D.L. Chung, Carbon Materials, World Scientific., 2019. Ch. 6.
[2] J. Chen, J.M. Wu, H.Y. Ge, D. Zhao, C. Liu, X.F. Hong, Reduced graphene oxide deposited carbon fiber reinforced polymer composites for electromagnetic interference shielding, Comp A 82 (2016) 141–150.
[3] Y. Bhattacharjee, V. Bhingardive, S. Biswas, S. Bose, Construction of a carbon fiber based layer-by-layer (LbL) assembly – a smart approach towards effective EMI shielding, RSC Adv. 6 (113) (2016) 112614–112619.
[4] M.G. Jang, S.C. Ryu, K.J. Juhn, S.K. Kim, W.N. Kim, Effects of carbon fiber modification with multiwall CNT on the electrical conductivity and EMI shielding effectiveness of polycarbonate/carbon fiber/CNT composites, J. Appl. Polym. Sci. 136 (14) (2019) 47302, 9.
[5] S.K. Vishwanath, D.G. Kim, J.H. Kim, Electromagnetic interference shielding effectiveness of invisible metal-mesh prepared by electrohydrodynamic jet printing, Jpn. J. Appl. Phys. 53 (5S3) (2014) 4, 05HB11.
[6] K. Chizari, M. Arjmand, Z. Liu, U. Sundararaj, D. Therriault, Three-dimensional printing of highly conductive polymer nanocomposites for EMI shielding applications, Mater Today Commun 11 (2017) 112–118.
[7] Y. Han, Y.X. Liu, L. Han, J. Lin, P. Jin, High-performance hierarchical graphene/metal-mesh film for optically transparent electromagnetic interference shielding, Carbon 115 (2017) 34–42.
[8] H.Y. Wang, Z.G. Lu, Y.S. Liu, J.B. Tan, L.M. Ma, S. Lin, Double-layer interlaced nested multi-ring array metallic mesh for high-performance transparent electromagnetic interference shielding, Opt. Lett. 42 (8) (2017) 1620–1623.
[9] D.D.L. Chung, A.A. Eddib, Effect of fiber lay-up configuration on the electromagnetic interference shielding effectiveness of continuous carbon fiber polymer-matrix composite, Carbon 141 (2019) 685–691.
[10] R. Rohini, S. Bose, Electrodeposited carbon fiber and epoxy based sandwich architectures suppress electromagnetic radiation by absorption, Composites, Part B 161 (2019) 578–585.
[11] S. Mishra, P. Katti, S. Kumar, S. Bose, Macroporous epoxy-carbon fiber structures with a sacrificial 3D printed polymeric mesh suppress electromagnetic radiation, Chem. Eng. J. 357 (2019) 384–394.
[12] L.C. Jia, L. Xu, F. Ren, P.G. Ren, D.X. Yan, Stretchable and durable conductive fabric for untrahigh performance electromagnetic interference shielding, Carbon 144 (2019) 101–108.
[13] S.S. Hwang, Tensile, electrical conductivity and EMI shielding properties of solid and foamed PBT/carbon fiber composites, Compos, Part B 98 (2016) 1–8.
[14] D. Micheli, S. Laurenzi, P.V. Mariani, F. Moglie, G. Gradoni, M. Marchetti, Electromagnetic shielding of oriented carbon fiber composite materials, in: Proc ESA Workshop on Aerospace EMC. Venice, IEEE, 2012, pp. 1–5.
[15] J.M. Yang, Y.Q. Yang, H.J. Duan, G.Z. Zhao, Y.Q. Liu, Light-weight epoxy/nickel coated carbon fibers conductive foams for electromagnetic interference shielding, J. Mater. Sci. Mater. Electron. 28 (2017) 5925–5930.
[16] D.D.L. Chung, Processing-structure-property relationships of continuous carbon fiber polymer matrix composites, Mater. Sci. Eng. R 113 (2017) 1–29.
[17] X. Luo, D.D.L. Chung, Electromagnetic interference shielding using continuous carbon fiber carbon-matrix and polymer-matrix composites, Compos Part B-Eng 30 (1999) 227–231.
[18] T.W. Shyr, J.W. Shie, Electromagnetic shielding mechanisms using soft magnetic stainless steel fiber enabled polyester textiles, J. Magn. Magn. Mater. 324 (2012) 4127–4132.
[19] H.J. Kim, S.H. Kim, S. Park, Effects of the carbon fiber-carbon microcoil hybrid formation on the effectiveness of electromagnetic wave shielding on carbon fibers-based fabrics, Mater 11 (2018) 2344, 14.
[20] L.S. Lu, D. Xing, Y.X. Xie, K.S. The, B. Zhang, S.M. Chen, et al., Electrical conductivity investigation of a nonwoven fabric composed of carbon fibers and polypropylene/polyethylene core/sheath bicomponent fibers, Mater. Des. 112 (2016) 383–391.
[21] G.H. Kang, S.H. Kim, Effect of incorporating carbon nanocoils on the efficiency of electromagnetic-wave shielding of carbon-nanomaterial composites, Appl. Surf. Sci. 380 (2016) 114–118.
[22] K.W. Kim, W. Han, B.S. Kim, B.J. Kim, K.H. An, A study on EMI shielding enhancement behaviors of Ni-plated CFs-reinforced polymer matrix composites by post heat treatment, Appl. Surf. Sci. 415 (2017) 55–60.
[23] J. Lee, Y. Liu, Y. Liu, S.J. Park, M. Park, H.Y. Kim, Ultrahigh electromagnetic interference shielding performance of lightweight, flexible, and highly conductive copper-clad carbon fiber nonwoven fabrics, J. Mater. Chem. C 5 (31) (2017) 7853–7861.
[24] C.Y. Liu, Z.X. Kang, Facile fabrication of conductive silver films on carbon fiber fabrics via two components spray deposition technique for electromagnetic interference shielding, Appl. Surf. Sci. 487 (2019) 1245–1252.
[25] L.C. Jia, L. Xu, F. Ren, P.G. Ren, D.X. Yan, Z.M. Li, Stretchable and durable conductive fabric for ultrahigh performance electromagnetic interference shielding, Carbon 144 (2019) 101–108.
[26] Y.C. Su, B.Y. Zhou, L.F. Liu, J.S. Lian, G.Y. Li, Electromagnetic shielding and corrosion resistance of electroless Ni-P and Ni-P-Cu coatings on polymer/carbon fiber composites, Polym. Compos. 36 (5) (2015) 923–930.
[27] J.T. Kim, C.W. Park, B.J. Kim, A study on synergetic EMI shielding behaviors of Ni-Co alloy-coated carbon fibers-reinforced composites, Synth. Met. 223 (2017) 212–217.
[28] S.H. Lee, J.Y. Kim, C.M. Koo, W.N. Kim, Effects of processing methods on the electrical conductivity, electromagnetic parameters, and EMI shielding effectiveness of polypropylene/nickel-coated carbon fiber composites, Macromol. Res. 9 (2017) 936–943.
[29] Z. Song, Z. Xia, J. Nie, Z. Tian, Improving the electrical and electromagnetic shielding properties of conductive silicon rubber filled with Ni-coated carbon fiber by magnetic field, Plast Rubber Comps 45 (2016) 224–228.
[30] A.A. Eddib, D.D.L. Chung, Radio-frequency linear absorption coefficient of carbon materials, its dependence on the thickness and its independence on the carbon structure, Carbon 124 (2017) 473–478.
[31] J.M. Kim, Y. Lee, M.G. Jang, C. Han, W.N. Kim, Electrical conductivity and EMI shielding effectivenessof polyurethane foam–conductive filler composites, J. Appl. Polym. Sci. 134 (5) (2017) 44373, 13.
[32] Teijin Carbon America, Inc., Private Communication.
[33] https://www.teijincarbon.com/fileadmin/PDF/Datenbl%C3%A4tter_en/Filament-Product_programm_EU_v27_2018-06-27_EN.pdf as viewed on Sept. 29, 2018.
[34] http://ase.au.dk/fileadmin/www.ase.au.dk/Filer/Laboratorier_og_vaerksteder/Komposit-lab/Fiber/Carbon/Carbon_UD_HS_194_gsm_Tenax-E_HTS45_E23-TDS.pdf as viewed on Sept. 22, 2018.
[35] http://pdf.directindustry.com/pdf/toho-tenax-europe-gmbh/tenax-e-hts45-p12-12k/37818-629937.html as viewed on Sept.22, 2018.
[36] X. Xi, D.D.L. Chung, Colossal electric permittivity discovered in polyacrylonitrile (PAN) based carbon fiber, with comparison of PAN-based and pitch-based carbon fibers, Carbon 145 (2019) 734–739.
[37] X. Xi, D.D.L. Chung, Piezoelectric and piezoresistive behavior of unmodified carbon fiber, Carbon 145 (2019) 452–461.
[38] X. Xi, D.D.L. Chung, Effect of nickel coating on the stress-dependent electric permittivity, piezoelectricity and piezoresistivity of carbon fiber, with relevance to stress self-sensing, Carbon 145 (2019) 401–410.
[39] B. Pierozynski, On the hydrogen evolution reaction at nickel-coated carbon fibre in 30 wt. % KOH solution, Int J Electrochem Sci 6 (2011) 63–77.
[40] https://en.wikipedia.org/wiki/Nickel as viewed on Dec. 28, 2018.
[41] N. Li, Y. Huang, F. Du, X.B. He, X. Lin, H.J. Gao, et al., Electromagnetic interference (EMI) shielding of single-walled carbon nanotube epoxy composites, Nano Lett. 6 (6) (2006) 1141–1145.
[42] M.S. Cao, J. Yang, W.L. Song, D.Q. Zhang, B. Wen, H.B. Jin, et al., Ferroferric oxide/multiwalled carbon nanotube vs polyaniline/ferroferric oxide/multiwalled carbon nanotube multiheterostructures for highly effective microwave absorption, ACS Appl. Mater. Interfaces 4 (12) (2012) 6949–6956.
[43] M.S. Cao, W.L. Song, Z.L. Hou, B. Wen, J. Yuan, The effects of temperature and frequency on the dielectric properties, electromagnetic interference shielding and microwave-absorption of short carbon fiber/silica composites, Carbon 48 (2010) 788–796.
[44] B. Wen, M.S. Cao, Z.L. Hou, W.L. Song, L. Zhang, M.M. Lu, et al., Temperature dependent microwave attenuation behavior for carbon-nanotube/silica composites, Carbon 65 (2013) 124–139.
[45] M. Ramirez, D.D.L. Chung, Electromechanical, self-sensing and viscoelastic behavior of carbon fiber tows, Carbon 110 (2016) 8–16.
[46] D. Wang, D.D.L. Chung, Through-thickness piezoresistivity in a carbon fiber polymer-matrix structural composite for electrical-resistance-based through-thickness strain sensing, Carbon 60 (1) (2013) 129–138.
[47] M.H. Al-Saleh, W.H. Saadeh, U. Sundararaj, EMI shielding effectiveness of carbon based nanostructured polymeric materials: a comparative study, Carbon 60 (2013) 146–156.
[48] L.X. Yin, X.Y. Tian, Z.T. Shang, X. Wang, Z.H. Hou, Characterization of continuous carbon fiber-reinforced composites for electromagnetic interference shielding fabricated by 3D printing, Appl. Phys. A 125 (11pp) (2019) 266.
[49] T. Tsutaoka, Frequency dispersion of complex permeability in Mn-Zn and Ni-Zn spinel ferrites and their composite materials, J. Appl. Phys. 93 (5) (2003) 2789–2796.
[50] Z.F. Zhang, W.H. Dang, C.J. Dong, G. Chen, Y.D. Wang, H.T. Guan, Facile synthesis of core–shell carbon nanotubes@MnOOH nanocomposites with remarkable dielectric loss and electromagnetic shielding properties, RSC Adv. 6 (2016) 90002–90009.
[51] Y. Zhang, Z.J. Yang, Y. Yu, B.Y. Wen, Y.Y. Liu, M.N. Qiu, Tunable electromagnetic interference shielding ability in a one-dimensional bagasse fiber/polyaniline heterostructure, ACS Appl Polym Sci 1 (2019) 737–745.
[52] https://en.wikipedia.org/wiki/Permeability_(electromagnetism) as viewed on Feb. 11, 2019.
[53] S. Celozzi, R. Aeaneo, G. Lovat, Electromagnetic Shielding, Wiley-IEEE Press, 2008.
[54] T.K. Gupta, B.P. Singh, V.N. Singh, S. Teotia, A.P. Singh, I. Elizabeth, et al., MnO_2 decorated graphene nanoribbons with superior permittivity and excellent microwave shielding properties, J. Mater. Chem. 2 (12) (2014) 4256–4263.
[55] D.X. Yan, H. Pang, B. Li, R. Vajtai, L. Xu, P.G. Ren, WangvJH, Z.M. Li, Structured reduced graphene oxide/polymer composites for ultra-efficient electromagnetic interference shielding, Adv. Funct. Mater. 25 (4) (2015) 559–566.
[56] X. Hong, D.D.L. Chung, Carbon nanofiber mats for electromagnetic interference shielding, Carbon 111 (2017) 529, 527.
[57] D. Wang, D.D.L. Chung, Through-thickness stress sensing of carbon fiber polymer-matrix composite by electrical resistance measurement, Smart Mater. Struct. 16 (2007) 1320–1330.